JOURNAL OF PROPULSION AND POWER
Vol. 26, No. 1, January–February 2010

High-Power Brayton Rotating Unit for Reactor and Solar Dynamic Power Systems

Mohamed S. El-Genk* and Bruno M. Gallo†
University of New Mexico, Albuquerque, New Mexico 87131

DOI: 10.2514/1.45409

The University of New Mexico Brayton Rotating Unit-3 (UNM-BRU-3), designed for 40 g/mole He-Xe working fluid, is optimized for shaft speed of 45 krpm, turbine and compressor inlet temperatures of 1149 and 400 K, and thermal power input of 157 kW_{th}. At these conditions, the electrical power and thermal efficiency are 54.2 kW_e and 34.5%, the compressor exit pressure is 1.044 MPa, the He-Xe flow rate is 1.54 kg/s, and the corresponding specific mass is 0.98 kg/kW_e. Investigated are the effects of decreasing the turbine inlet temperature to 900 K and the thermal power input to 40 kW_{th} and varying the shaft speed from 30 to 55 krpm. At 900 K turbine inlet temperature, thermal power input of 157 kW_{th}, and shaft rotation speed of 45 krpm, the UNM-BRU-3 has a thermal efficiency of 22.8% and generates 34.2 kW_e at a compressor exit pressure of 1.3 MPa and He-Xe flow rate of 2.07 kg/s; but the specific mass of the unit increases to ~1.55 kg/kW_e. The unit performance at 900 K is attractive for early deployment of space reactor and solar dynamics power systems with stainless steel structure, thus minimizing development cost and enhancing operation reliability and life. The low specific mass of UNM-BRU-3 will reduce the total mass and launch cost of these systems.

Nomenclature

A	=	electrical alternator
C	=	compressor
M	=	molecular weight, g/mole
m	=	mass, kg
$\dot{m}$	=	mass flow rate, kg/s
P	=	pressure, Pa
P_e	=	electrical power, kW_e
Q_{Sec}	=	Brayton rotating unit thermal power, $Q_{th}/3$, kW
Q_{th}	=	reactor thermal power, kW
T	=	temperature, K, turbine
V	=	actual gas velocity, m/s; voltage, V
W	=	work rate, kW
x	=	bled fraction of closed-Brayton-cycle working fluid
α	=	actual gas flow angle, deg
β	=	geometrical blade angle, deg
δ	=	deflection angle, deg; gap, m
η	=	efficiency, %
π	=	pressure ratio

Subscripts

A	=	alternator
BRU	=	Brayton rotating unit
C	=	compressor
G	=	electrical generator, or alternator
GC	=	gas cooler
loss	=	energy losses
o	=	reference value, 273.16 K, compressor inlet
Rx	=	reactor
shaft	=	rotating shaft
SYS	=	power system
T	=	turbine
0	=	total thermodynamic or stagnation
1, (1)	=	compressor inlet
2	=	compressor diffuser inlet
(3)	=	reactor inlet
3, (2)	=	compressor exit
4, (4)	=	turbine inlet
5	=	turbine stator exit
6	=	turbine rotor inlet
(6)	=	gas cooler inlet
7, (5)	=	turbine exit

Superscripts

C	=	compressor
T	=	turbine

Received 12 May 2009; accepted for publication 8 September 2009.

*Regents' Professor of Chemical, Nuclear, and Mechanical Engineering, and Director, Institute for Space and Nuclear Power Studies, School of Engineering, MSC01 1120, 1. Associate Fellow AIAA.

†Graduate Research Assistant, Chemical and Nuclear Engineering Department and Institute for Space and Nuclear Power Studies, MSC01 1120, 1.

I. Introduction

BRAYTON rotating units (BRUs) had been considered for use in both radioisotope and reactor space power systems as well as dynamic solar power systems. These systems were designed for a relatively high thermal efficiency using one or multiple closed-Brayton-cycle (CBC) loops [1–4]. In the 1970s, NASA had designed and successfully tested several BRUs with induction magnet alternators at the John H. Glenn Research Center at Lewis Field. Some of these BRUs have been tested for more than 36,000 h in a simulated space environment at a turbine inlet temperature of 1144 K, without degradation [1]. BRUs for generating to 10.5 kW_e have also been designed, built, and tested successfully by NASA for tens of thousands of hours at a shaft speed of 36 krpm [2]. A 35 kW_e BRU, also with an induction magnet alternator and for a nominal rotating shaft speed of 32 krpm, had been developed for use with a radioisotope heat source and in solar dynamic power systems [3,4]. Recently, there has been an interest in developing high-power BRUs (20–50 kW_e) for uses in space reactor power systems for high-power electric propulsion in support of future interplanetary missions [5–9].

The type and molecular weight of the CBC gas working fluid affect not only the thermal efficiency, but also the design, performance, and size of the BRU [10]. A typical BRU consists of a centrifugal-flow compressor and a radial-inflow turbine mounted on single shaft with the electrical alternator [5,7,10]. The shaft rotation speed could be as much as 45 krpm, or even higher. For a space power

system with direct CBC, the BRU working fluid is also the coolant of the heat source, being solar or a compact fission reactor.

Space reactor power systems with one or multiple, direct CBCs are relatively compact with a plausible specific mass ≤ 50 kg/kW$_e$. This specific mass includes the nuclear reactor heat source, the radiation shadow shield, the BRUs, piping, recuperator and gas cooler, the reactor instrumentation and control, the support structure, the liquid metal secondary loop, and the water heat pipes radiator panels (e.g., Fig. 1). Space reactor power systems with CBCs could support interplanetary exploration missions and Mars and lunar outposts, where the solar option is impractical or nonexistent. These power systems are currently the only option for high electrical power for these and other space missions. They are capable of generating tens to hundreds of kW$_e$ continuously for 10 years, or even longer. The electric power generated by these systems could also be used to operate plasma thrusters for high specific impulse propulsion (5000–15,000 s), shortening the travel time to distant planets in the solar system.

Closed-Brayton-cycle energy conversion is suitable with a gas-cooled nuclear reactor or solar heat source [11–13]. The thermal efficiency of a space reactor power system with CBC for energy conversion could be in excess of 20%, and as much as 35%, depending on the reactor thermal power, the BRU design, inlet temperature to the BRU turbine, the type and molecular weight of the gas working fluid, and the rotating shaft speed.

Space reactor power systems with CBCs typically use binary gas mixtures of He-Xe with molecular weights of 15–40 g/mole, both as reactor coolant and CBC working fluid. In addition to their inertness, the He-Xe gas mixture with a 15 g/mole has ~7% higher heat transfer coefficient than pure helium, while that of 40 g/mole has the same heat transfer coefficient as helium [10]. These He-Xe binary gas mixtures significantly decrease the aerodynamic loading of the compressor impeller and the turbine blades to only ~27.7% and 10% of those with helium, but increase the pressure losses in the CBC loop [10]. With the 40 g/mole He-Xe working fluid and reactor coolant (Fig. 1), the pressure losses in the CBC loop could be as much as 6.5 times those with helium, requiring larger diameter piping and flow channels in the recuperator, gas cooler, and the nuclear reactor (e.g., Fig. 1). However, because compactness and low mass are primary design drivers for space reactor power systems, the He-Xe binary mixture with a molecular weight of 40 g/mole has been the preferred working fluid for high-power BRUs for space applications [10]. To further enhance the performance of the reactor power system, the BRUs employ electrical alternators with permanent magnets that are passively cooled using an auxiliary heat pipes radiator (e.g., Fig. 1). The low mass and the high efficiency of these alternators effectively increase the power system's electrical power and thermal efficiency and decrease its specific mass (or alpha).

A gas-cooled, fission reactor heat source could be hydraulically coupled directly to one CBC loop or more. To avoid single point failures in reactor cooling and energy conversion, the Submersion-Subcritical Safe Space ($S^\wedge4$) reactor with a sectored core [12] could be used (e.g., Fig. 1). The gas-cooled reactor core consists of three identical sectors that are thermally and neutronically coupled, but hydraulically decoupled. Each sector has its own CBC loop and a separate BRU and separate heat rejection radiator panels (Fig. 1) [11–13]. Thus, with a failure or a pipe break in one of the CBC loops, the thermal power of the $S^\wedge4$ reactor is reduced with the other two CBC loops continuing to operate, but at lower electrical power and lower thermal efficiency. The fission power generated in the reactor sector of the failed CBC will be conducted to the adjacent two sectors and removed by the circulating He-Xe gas coolant in these sectors.

The reported performance analyses of space reactor power systems with direct CBCs for energy conversion, such as that in Fig. 1, have solely been based on using simplified thermodynamic models of the CBC loop [9]. The input to these models includes constant inlet pressures and temperatures and polytropic efficiencies of the BRU turbine and the compressor, constant shaft mechanical losses, and constant electrical alternator efficiency and recuperator effectiveness. Thus, the performance predictions of these models are independent of the design and rotation speed of the BRU shaft and the operation characteristics of the turbine and compressors, which depend on the turbine inlet temperature, the rotation speed of the BRU shaft, and the type and molecular weight of the CBC working fluid. Some of these models also assume or neglect the pressure and thermal losses in the piping and other CBC components. Thus, thermodynamic models, though useful as a first cut, could not be used to quantify the effects on the system performance of changing the design of the BRU compressor and turbine, the rotating speed of the BRU, the type and the molecular weight of the working fluid, the turbine and compressor inlet temperatures, the thermal power input to the BRU turbine, and the heat rejection radiator design. To account for these effects, detailed design and performance models of the turbine, compressor, and the integrated BRU have been developed and validated, before being coupled to a thermodynamic model of a space reactor power system with CBC loops for energy conversion (e.g., Fig. 1) [11,14].

This paper presents the developed design and the performance results of the high-power New Mexico Brayton Rotating Unit-3 (UNM-BRU-3) optimized for 40 g/mole He-Xe gas working fluid, shaft rotation speed of 45 krpm, compressor inlet temperature of 400 K, and turbine inlet temperature and thermal power input Q_{Sec}, of 1149 K and 157 kW$_{\text{th}}$. In addition to developing and optimizing the hardware of the turbine and the compressor, the contribution of this work includes developing and validating the developed performance models for the compressor and the turbine, as well as of the rotating

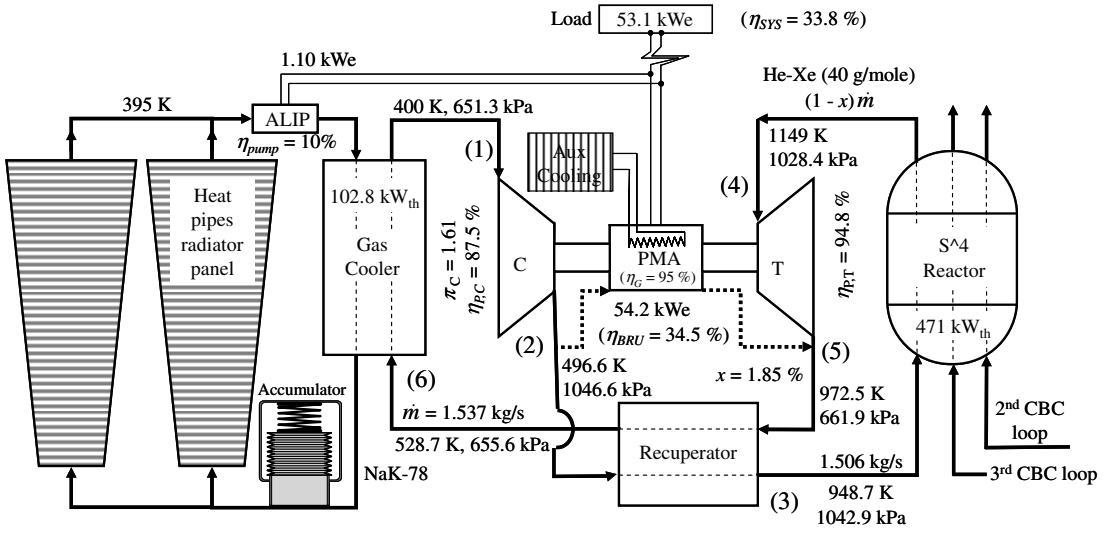

Fig. 1 Nominal operation parameters of space power system with an $S^\wedge4$ reactor heat source and three CBC loops each with a UNM-BRU-3.

shaft. These models are then coupled with the electrical alternator to calculate the performance of the integrated UNM-BRU-3. The UNM-BRU-3 employs an alternator with a cobalt-samarium permanent magnet. Recognizing that the core and joules losses in the electrical alternator change with the shaft speed and the applied electrical load and many other parameters, a detailed model of the electrical alternator needs to be developed to account for all these effects. This, however, is outside the original scope of this paper. Instead, a constant efficiency of 95% is assumed for the permanent magnet alternator (PMA) in the UNM-BRU-3. This efficiency is the average of the values reported for these types of alternators (93–96%) [14,15].

This paper also investigates the effects on the performance of the UNM-BRU-3 of changing the shaft rotation speed from 30 to 55 krpm and the thermal power to the BRU turbine from 40 to 157 kW_{th}, and of decreasing the turbine inlet temperature from 1149 to 900 K. In the present performance analysis of the UNM-BRU-3, the physical and transport properties of the He-Xe working fluid (40 g/mole) are determined as functions of pressure and temperature [10]. The developed design and performance models of the compressor and turbine in the UNM-BRU-3 are validated using reported data for a number of NASA units developed and tested in the 1960s and 1970s [16,17].

The thermal efficiency and the electrical power of the UNM-BRU-3, when operating at a turbine inlet temperature of only 900 K, are very attractive for future development of space nuclear reactor power systems. At such a relatively low turbine inlet temperature, stainless steel could be used for the reactor structure, fuel cladding, and the CBC loop piping and components. In addition to decreasing the time to deployment of the power system, using stainless steel, with well-known properties and extensive operation experience, will enhance the system's reliability and safety and effectively reduce the total cost of construction and launch. Issues regarding the structural integrity and potential creep of the rotor and the containment of the electrical alternator and of the mechanical members of the UNM-BRU-3, though very important and should be addressed in a follow-up effort, are outside the scope of this work.

II. Compressor and Turbine Performance Models

The developed performance models of the compressor and turbine of the UNM-BRU-3 (Figs. 2 and 3) use a mean flow approach [14,18–30] and solve the coupled state equation and the overall mass, energy, and momentum conservation equations of the gas working fluid in all stages, subject to the appropriate inlet and exit flow conditions. In addition to accounting for the various energy and pressure losses in all stages, these models track the gas flow along a mean streamline in the different stages of the turbine and compressor (Figs. 3a and 3b). Each compressor and turbine stage experiences different enthalpy changes as well as losses. The enthalpy losses are calculated as a function of the blade geometry, the hardware dimensions, the gas local velocity, and thermodynamic and transport properties [21–32]. All thermodynamic properties of the He-Xe gas

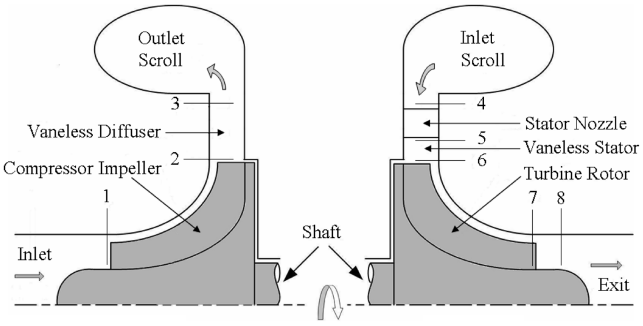

a) Compressor **b) Turbine**

Fig. 2 Fluid flowpaths in various stages of the compressor and turbine in a CBC turbomachine unit.

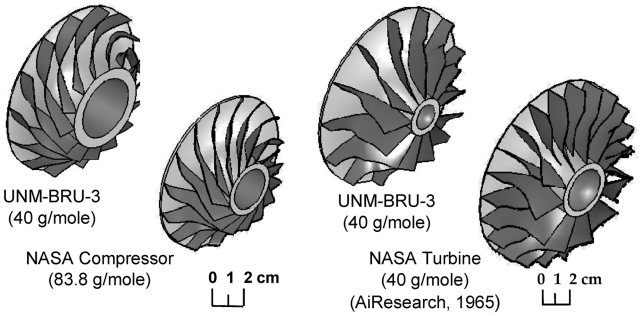

a) UNM-BRU-3 compressor **b) UNM-BRU-3 turbine**

Fig. 3 Solid models of NASA compressor and turbine rotors [16] and those of the 54.2 kW_e UNM-BRU-3.

working fluid (40 g/mole) in various stages of the compressor and turbine (Figs. 2a and 2b) are evaluated at the local bulk temperature and pressure.

The coupled governing equations of the gas working fluid are solved for the state variables at the exit of each stage in the turbine and the compressor, in terms of those at the stage's inlet or the exit of the prior stage. The flow areas at the entrance and exit of each stage in the turbine and the compressor are calculated from the dimensions of the developed hardware for the turbine and the compressor (Fig. 3). These dimensions and input parameters include the radii of the compressor impeller and turbine blades, the blades' angles and thicknesses, the number of blades, and the width and height of the flow passages (e.g., Table 1). Before investigating the performance of the UNM-BRU-3, the developed turbine and compressor models are validated for a number of NASA turbine and compressor designs that used different working fluids. The validation results of the present compressor and turbine models are presented and discussed next.

A. Validation of the Compressor and Turbine Models

During the 1960s and 1970s, many BRU designs had been developed, built, and tested for NASA. Some of these units had been tested for more than 36,000 h by AiResearch (now Honeywell International, Inc., and formerly AlliedSignal, Inc.) in a simulated space environment and at turbine inlet temperature of 1144 K at the NASA John H. Glenn Research Center at Lewis Field, without a performance degradation [17]. Each of these BRUs consists of a centrifugal-flow compressor, a radial-inflow turbine, an induction magnet alternator, and a gas bearing system, all mounted onto a single shaft. The tested BRU designs had used different working fluids of krypton, argon, air, and He-Xe binary mixtures [17,16]. The reported design and input parameters used to validate the present models for the BRU compressor [16], the Eckardt compressor O [33–35], and the BRU turbine [18] are listed in Table 1. The reported test data for these compressors and turbine [16,33–35] are compared in Tables 2 and 3 with the predictions of the present compressor and turbine models, using the same working fluids in the tests.

The design and performance parameters used to benchmark the predictions of the present compressor model are of a compressor that had a diameter of 10.8 cm and used He-Xe binary mixture working fluid with a molecular weight of 83.8 g/mole (same as that of argon) [16]. This compressor operated at a shaft rotation speed of 36 krpm. The calculated performance for this compressor (first column in Table 1) by the present compressor model is for mass flow rate of the gas working fluid, $\dot{m} = 0.36145$ kg/s, and inlet temperature of 300 K. The hardware details and the reported performance parameters of this compressor are listed in Table 1 and the reported performance data are compared with the present calculations in Table 3 [16].

In addition, the reported performance data of three centrifugal compressors developed and tested at the Institut für Luftstrahlantriebe in the 1970s (impellers O, A, and B [33,34]), are used to validate the predictions of the present compressor model. The impeller O (third column in Table 1) had a discharge radius of 40 cm

Table 1 Compressor and turbine designs and operation parameters for benchmarking present models

Parameter	Compressor [16]	Turbine [16]	Impeller O [33]
Blade thickness, mm	1.5	2.2	1
Number of full/split blades	15/NA	11/11	20/NA
Number of stator blades	NA	14	NA
Nozzle angle at stator inlet $\beta_{4,\text{nozzle}}$, deg	NA	55.6	NA
Nozzle angle at stator exit, $\beta_{5,\text{nozzle}}$, deg	NA	78	NA
Blade angle at impeller inlet $(\beta_1)/(\beta_6)$, deg	39.4	1.125	35
Blade angle at impeller exit $(\beta_2)/(\beta_7)$, deg	58.9	50.8	90
Absolute gas angle at impeller inlet, deg	90	NA	90
Stator inlet/exit radius, mm	NA/NA	96/78.4	NA/NA
Radius at compressor inlet r_o, mm	48.82	NA	140
Hub radius at compressor inlet (r_1)/turbine exit (r_6), mm	18.29	19.1	45
Shroud radius at compressor inlet/turbine exit, mm	33.1	54.33	140
Impeller radius at compressor exit/turbine inlet, mm	53.98	76.2	200
Diffuser exit radius, mm	83.2	NA	400
Impeller blade height at compressor exit/turbine inlet, mm	5.2	19.185	26
Nozzle blade chord, mm	NA	46	NA
Working fluid	He-Xe	Ar	Air
Molecular weight, g/mole	83.8	39.9	28.9
Total inlet pressure, kPa	93.08	90.66	101.325
Total inlet temperature, K	300	1083.3	288.1
Mass flow rate, kg/s	0.36145	0.2774	5.31
Shaft angular speed, krpm	36	38.5	14

Table 2 Comparison of turbine model with reported data for the NASA BRU turbine

Parameter	NASA BRU turbine [16]	Present model	Diff., %
Pressure ratio, π_T	1.531	1.553	1.42
Isentropic efficiency, %	88.6	88.68	0.1
Total enthalpy losses, kJ/kg	10.41	10.49	0.78
Exit velocity from rotor, m/s, V_7	137.5	134.3	2.29
Rotor exit total pressure, kPa, P_{07}	56.40	55.68	1.27
Rotor exit total temperature, K, T_{07}	910.2	907.9	0.25
Inlet velocity to rotor, m/s, V_6	282.8	282.4	0.13
Rotor inlet flow angle, deg, α_6	−0.76	0.9	——
Rotor inlet total pressure, kPa, P_{06}	74.39	74.68	0.38
Rotor inlet total temperature, K, T_{06}	1006.5	1006.7	0.03

Table 3 Comparison of compressor model with reported data for NASA BRU compressor

Parameter	NASA BRU compressor [16]	Present model	Diff., %
Pressure ratio, π_C	2.096	2.016	0.67
Isentropic efficiency, %	89.8	90.3	0.51
Total enthalpy losses, kJ/kg	2.76	2.648	4.06
Compressor power, $\dot{W}_C$, kW	9.347	9.327	0.21
Impeller exit total pressure, kPa, P_{02}	144.0	143.0	0.71
Impeller exit total temperature, K,	366.7	367.5	0.20
Exit velocity at impeller, m/s, V_2	144.78	144.62	0.11
Exit flow angle, α_2, deg	22.1	22.47	1.67

and was coupled to a vaneless diffuser, 80 cm in diameter. The reported test parameters in Table 1 include the shaft rotational speed of 14 krpm, air working fluid flow rate of 5.31 kg/s, inlet pressure and temperature of 101.325 kPa and 288.1 K, total pressure ratio of 2.08, and isentropic efficiency of 88 %.

The reported performance data used to validate the predictions of the present turbine model (Table 2) are for a turbine that had a diameter of 15.2 cm, used argon working fluid, and operated at 38.5 krpm (second column in Table 1) [16]. It generated 22.3 kW of shaft mechanical power at an isentropic efficiency of 88%, when tested at inlet pressure and temperature of 83.39 kPa and 1072.3 K, mass flow rate of 0.2774 kg/s, and total pressure ratio of 1.56. As indicated in Tables 2 and 3, the differences between the predictions of the present models and the reported data for the BRU compressor and turbine [16] are within a fraction to a few percents. Thus, the comparisons with the reported performance data of the various NASA BRU compressor and turbine [16] in Tables 2 and 3 confirm the soundness and the accuracy of the results of the present compressor and turbine models.

The validated compressor and turbine models, and a detailed model of the rotating shaft, are integrated to obtain the present BRU model [14]. The model of the BRU rotating shaft accounts for various losses and calculates the shaft mechanical efficiency as a function of the rotation speed [Eq. (4)]. The integrated BRU model is used in the next section to investigate the performance of the UNM-BRU-3 with advanced blades designs for the compressor and the turbine (Fig. 3).

B. Integrated Closed-Brayton-Cycle Model

Figures 3a and 3b compare the relative sizes of the rotors of NASA BRU compressor and turbine [16] to those of the UNM-BRU-3. The performance model of the BRU couples the compressor and turbine models to that of the rotating shaft model [14]. The hardware details and the dimensions of the compressor and turbine rotors in the

UNM-BRU-3 are optimized for operating at peak efficiency when the shaft speed is 45 krpm, the compressor inlet temperature is 400 K, and the turbine inlet temperature and thermal power are 1149 K and 157 kW_{th}, respectively. The efficiency of the UNM-BRU-3 electrical alternator with a cobalt-samarium permanent magnet η_G is assumed constant 95%; this value is the average of those reported by the manufactures of these types of alternators (93–96%) [15]. In addition to being lighter, this alternator is more efficient than those with induction magnets ($\eta_G < 90\%$) employed in the earlier NASA BRU designs [2–6,36].

In addition to the hardware details and dimensions of the compressor, turbine, rotating shaft, and the electrical alternator efficiency η_G, the input to the integrated UNM-BRU-3 model specifies the compressor and turbine inlet temperatures, the shaft rotational speed, the mass flow rate of the He-Xe (40 g/mole) working fluid, and the thermal power input to the turbine (Q_{sec}) (e.g., Fig. 1). The calculated parameters by the present BRU model include the shaft mechanical efficiency [14], the BRU electric power and thermal efficiency, the pressure ratio and polytropic efficiency of the compressor and turbine, and the state parameters at the different points in the CBC loop (Fig. 1). The electric power generated by the UNM-BRU-3 is calculated as

$$P_{e,\mathrm{BRU}} = \eta_{\mathrm{shaft}}\eta_G(W_T - W_C) \tag{1}$$

The thermal efficiency of the UNM-BRU- 3 is calculated as

$$\eta_{\mathrm{BRU}} = [P_{e,\mathrm{BRU}}/Q_{\mathrm{sec}}] = [(\eta_{\mathrm{shaft}}\eta_G(W_T - W_C))/Q_{\mathrm{sec}}] \tag{2}$$

The shaft mechanical efficiency is calculated as a function of the shaft rotation speed as [14]

$$\eta_{\mathrm{shaft}} = \left(1 - \frac{W_{\mathrm{shaft,loss}}}{(W_T - W_C)}\right) \tag{3}$$

The turbine and the compressor powers W_T and W_C, as well as the shaft losses $W_{\mathrm{shaft,loss}}$, depend on the rotation speed of the common shaft in the UNM-BRU-3. The rotating shaft losses W_{loss} are calculated [14] as the sum of four quantities: the thrust bearing losses W_{thrust}, the turbine and compressor disk windage losses W^T_{disk} and W^C_{disk}, and the shaft mechanical losses W_{shaft}, as [22,30–32]

$$W_{\mathrm{shaft,loss}} = (W_{\mathrm{thrust}} + W^T_{\mathrm{disk}} + W^C_{\mathrm{disk}} + W_{\mathrm{shaft}}) \tag{4}$$

C. Brayton Rotating Unit Electrical Alternator

Early BRU designs developed for NASA used brushless, nonrotating coil synchronous and three-phase Rice-Lundell alternators (RLAs). An RLA consists of high-strength brazed rotor and stator winding [37–39]. The output voltage is controlled within a specified range by regulating the induced magnetic field in the coil, regardless of the shaft speeds [15]. The rotor material (SAE 4340 and Inconel 718) allowed operation at up to 700 K [37,38]. The RLAs had been used in the 10.5 kW_e NASA BRU [10,18], the 2 kW_e mini-BRU [29], and the 35 kW_e Space Station Freedom BRU [4,38]. These alternators are no longer manufactured and have been replaced by more efficient and lighter synchronous alternators with permanent magnets [40].

The permanent magnet alternator typically uses alnico or cobalt-samarium magnet (Fig. 4) mounted onto the stator to generate the magnetic field [39–42]. Because the generated magnetic field is almost constant so long as the magnet temperature is kept constant using passive cooling (e.g., Fig. 1), the output voltage could vary by ~10%, as either the electric load or the shaft rotational speed changes [37,40]. A voltage regulator is typically used to limit such changes in the output voltage to less than 10% [42]. The permanent magnet is cooled well below its curie point (Fig. 4). This is accomplished in a space reactor power system using an auxiliary heat pipes radiator (e.g., Fig. 1).

The desirable operation temperature of the permanent magnet is dictated by its material. For the cobalt-samarium, this temperature is ~500 K, which corresponds to 90% of the saturation magnetic flux,

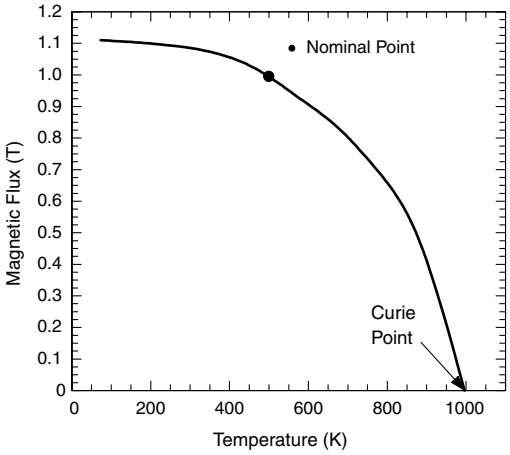

Fig. 4 Relationship between the cobalt-samarium magnetization and temperature [40].

and also much lower than the curie point of the cobalt-samarium magnet (996 K). The PMAs have high efficiency (93–96%) because of the short path of the magnetic field. Conversely, RLAs have lower efficiency (89–92%) due to the longer magnetic field paths and the joules losses in the magnetic field coil [36]. In addition to the high efficiency, PMAs have higher specific powers of 5–7 kW_e/kg than RLAs (3–5 kW_e/kg). The high specific power and efficiency of the PMAs make them a suitable choice for BRUs for space nuclear reactor power systems [40,43–46].

III. Results and Discussion

The performance results of the UNM-BRU-3 for He-Xe working fluid of 40 g/mole and with a PMA are presented and discussed in this section. These results are for the same conditions as when the BRU is integrated into the CBC loop(s) of a space reactor power system (Fig. 1). Thus, for the specified compressor and turbine inlet temperatures, the shaft rotation speed, and the input thermal power input to the BRU turbine, the mass flow rate of the He-Xe working fluid and the values of other thermodynamic parameters for the power system (Fig. 1) are calculated using the thermodynamic mode of the CBC loop. These thermodynamic parameters include the polytropic efficiencies, pressure ratios, and the inlet pressure and the exit pressure and temperature of the BRU turbine and the compressor (Figs. 5 and 6). The performance model of the integrated UNM-BRU-3 calculates the shaft mechanical efficiency and net mechanical power, and both the thermal efficiency η_{BRU} and electrical power P_e of the BRU.

The UNM-BRU-3 has a nominal peak thermal efficiency and peak electrical power of 34.5% and 54.2 kW_e, when operating at compressor and turbine inlet temperatures of 400 and 1149 K, shaft rotation speed of 45 krpm, and thermal power input to the turbine, $Q_{\mathrm{sec}} = 157$ kW_{th}. The present analyses varied several operation parameters, independently. These are the shaft rotation speed from 30 to 55 krpm, increasing the mass flow rate of the He-Xe working fluid from 0.38 to 3.6 kg/s, the thermal power supplied to the UNM-BRU-3 turbine by the working fluid from 40 to 157 kW_{th}, and the turbine inlet temperature $T_{(4)}$ from 900 to 1149 K. In the performance analyses of the UNM-BRU-3, the inlet temperature to the compressor $T_{(1)}$ is kept constant at 400 K (Fig. 1).

Although the comparison results with the reported test data for the NASA units confirm the soundness of the present compressor and turbine models, the accuracy of the results at the various parameters investigated in the paper (Figs. 7 and 8) would need to be confirmed with test results when available. The results of the parametric analysis assess the effects of various operation parameters on the overall performance of the UNM-BRU-3. Also, showing that designing nuclear reactor and solar dynamics power systems with CBC energy conversion could be done at low enough temperature (900 K) and still achieve good performance is an important finding. It

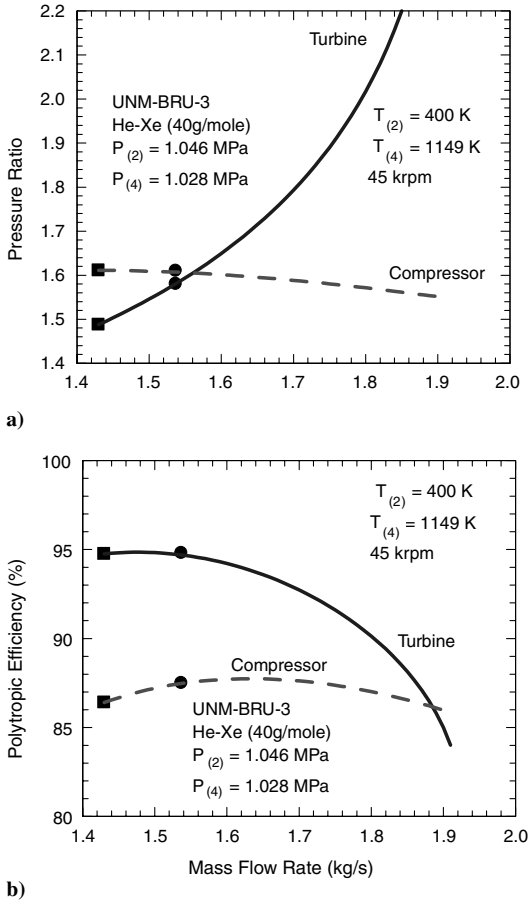

Fig. 5 Polytropic efficiency and pressure ratio for the UNM-BRU-3 compressor and turbine.

is also a critical point, because at such temperature, conventional steel structure could be used, reducing the development cost and time. The calculated polytropic efficiencies and pressure ratios of the turbine and the compressor of the UNM-BRU-3, when operating at compressor and turbine inlet temperatures of 1149 and 400 K, shaft speed of 45 krpm, and thermal power input to the turbines of 157 kW_{th} are presented (Figs. 5a and 5b) and discussed next.

A. Compressor and Turbine Polytropic Efficiencies

In Figs. 5a and 5b, the solid square symbols indicate the surge limit of the compressor, and the solid circle symbols indicate the nominal operating point of the UNM-BRU-3 at the peak thermal efficiency and peak electrical power. This is when the turbine inlet temperature and thermal power are 1149 K and 157 kW_{th} and the shaft speed is 45 krpm. The pressure ratio of the compressor decreases very little, whereas that of the turbine increases precipitously as the flow rate of the He-Xe working fluid (40 g/mole) (or the thermal power input to the BRU turbine Q_{sec}) increases (Fig. 5a).

At the nominal operation point of the UNM-BRU-3, at which the designs of the turbine and the compressor are optimized, the flow rate of the He-Xe working fluid is 1.54 kg/s and the pressure ratio of the compressor (1.605) is slightly higher than that of the turbine (1.58) (Fig. 5a), but, as shown in Fig. 5b, the polytropic efficiency of the turbine (94.8%) is significantly higher than that of the compressor (87.48%). The polytropic efficiency of the UNM-BRU-3 turbine initially increases slightly with increasing the flow rate of the He-Xe (40 g/mole) working fluid to reach a peak of 94.8% at ~1.49 kg/s, then drops fast with further increase in the flow rate of the working fluid (Fig. 5b), due to the increase in the enthalpy losses in the various stages of the turbine [14].

As shown in Fig. 6a, the polytropic efficiency of the compressor increases initially more notably with increasing the flow rate of the He-Xe working fluid to reach a peak of 87.7% at ~1.64 kg/s, then decreases with further increase in the flow rate (Fig. 5b). In Figs. 5a and 5b and in subsequent figures, the inlet pressures to the UNM-BRU-3 turbine and compressor $P_{(4)}$ and $P_{(2)}$, respectively, are kept constant and equal to those of the UNM-BRU-3 when nominally operating at $T_{(4)} = 1149$ and $T_{(2)} = 400$ K in the CBC loop, shaft speed of 45 krpm, and thermal power input to the turbine of 157 kW_{th} (Fig. 1).

Although the peak polytropic efficiencies of the UNM-BRU-3 turbine and the compressor correspond to different flow rates of He-Xe working fluid (Fig. 5b), the thermal efficiency of the UNM-BRU-3 peaks at the flow rate indicated by the solid circle symbols in Figs. 5a and 5b (1.54 kg/s). This flow rate is for a shaft rotation speed of 45 krpm and input thermal power to the turbine of 157 kW_{th}.

The peak polytropic efficiencies of the turbine and the compressor and the flow rates of the working fluid at which they occur depend on

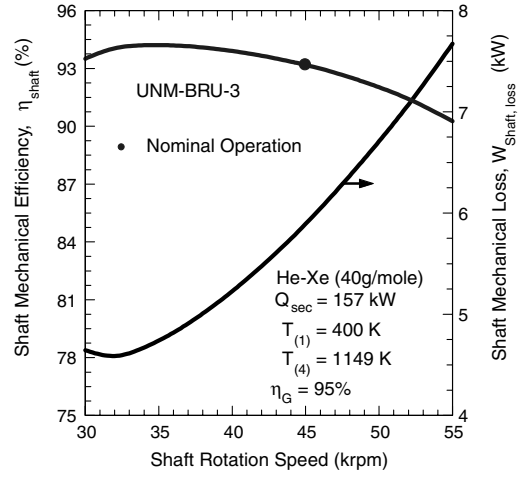

Fig. 6 Mechanical losses and efficiency of the UNM-BRU-3 shaft.

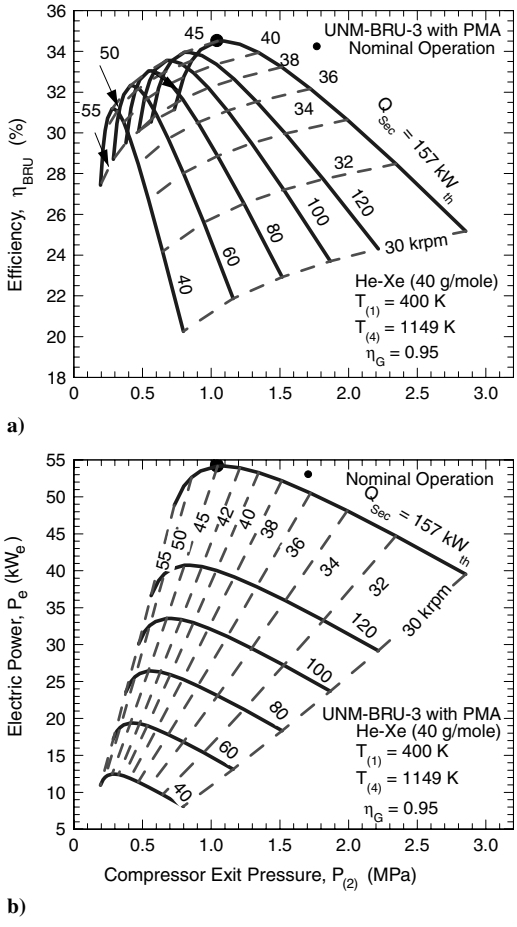

Fig. 7 Operation surfaces of the UNM-BRU-3.

the shaft rotation speed. Increasing (or decreasing) the shaft speed, decreases (or increases) the polytropic efficiencies of the turbine and the compressor at low flow rates, but increases (or decreases) them at higher flow rates. The mechanical efficiency of the UNM-BRU-3 shaft [14] increases initially as the shaft speed increases and peaks at 94.2% when the rotation speed is ~35 krpm. It then decreases with further increase of the shaft rotation speed. At the nominal operation speed of the UNM-BRU-3 (45 krpm), the shaft mechanical efficiency is 93.2% (Fig. 6). This efficiency accounts for various losses [Eq. (4)], namely, the thrust bearing losses, the compressor and turbine disk windage losses, and the shaft mechanical losses [14].

B. Brayton Rotating Unit Performance Results

The calculated performance parameters of the UNM-BRU-3 include the thermal efficiency (Fig. 7a) and the electrical power (Fig. 7b). The latter assumes PMA efficiency, $\eta_G = 95\%$, and takes into account the change in the mechanical efficiency of the BRU shaft with the rotation speed, but not the changes in the alternator losses with the shaft speed (Fig. 6) [14]. It is worth noting that both the core and joules losses in the electrical alternator and hence, its efficiency, change with the rotation speed of the shaft and should be taken into consideration. However, this is outside the scope of the present work, focusing on the mechanical design of a high-performance BRU, for which the calculated net mechanical power of the shaft accounts for the shaft's mechanical losses and the enthalpy losses in the turbine and the compressor.

Figure 7a presents the operation surface of the thermal efficiency of the UNM-BRU-3. It is a grid constructed of constant turbine input thermal power lines ($Q_{sec} = 40$–157 kW_{th}) and intersecting lines of constant shaft rotation speed (30–55 krpm). The values of the UNM-BRU-3 thermal efficiency in Fig. 7a account for the shaft mechanical losses and 5% losses in the electrical generator ($\eta_G = 95\%$), but neglects the thermal losses from the outside surface of the reactor vessel and of the CBC piping and components, which are assumed to be well insulated. Similarly, Fig. 7b presents the corresponding operation surface for the UNM-BRU-3 electrical power. The results in Figs. 7a and 7b are for steady-state operation at constant turbine inlet temperature of 1149 K and compressor inlet temperature of 400 K (Fig. 1).

Figure 7a shows that increasing the shaft rotation speed beyond 45 krpm decreases the thermal efficiency and the electrical power of the UNM-BRU-3 as well as the compressor exit pressure $P_{(2)}$. On the other hand, decreasing the shaft rotation speed below 45 krpm decreases the thermal efficiency and the electrical power of the UNM-BRU-3, but increases the compressor's exit pressure. For the same shaft speed, decreasing the thermal power input to the turbine Q_{sec}, decreases the thermal efficiency, the electrical power, and the compressor exit pressure of the UNM-BRU-3. However, the effect of decreasing the shaft rotation speed on the electrical power of the UNM-BRU-3 (Fig. 7b) is much less than on the thermal efficiency (Fig. 7a).

At a thermal power input to the turbine Q_{sec} of 157 kW_{th} and shaft rotation speed of 45 krpm, the calculated thermal efficiency of the UNM-BRU-3 is 34.5% and the pressure at the exit of the compressor is $P_{(2)} = 1.04$ MPa (Fig. 7a). At the same thermal power input to the turbine, decreasing the shaft rotation speed to 40 krpm, decreases the thermal efficiency of the UNM-BRU-3 slightly to 33.94%, while increasing the compressor's exit pressure $P_{(2)}$ to 1.35 MPa. Further decrease in the shaft rotation speed to 30 krpm, while keeping the thermal power input to the turbine constant at 157 kW_{th}, decreases the thermal efficiency of the UNM-BRU-3 to 25.2% and increases the compressor's exit pressure to as much as 2.85 MPa (Fig. 7a). These results clearly show that decreasing the shaft speed significantly decreases the thermal efficiency and, to a lesser extent, the electrical power of the UNM-BRU-3. Conversely, decreasing the thermal power input to the turbine significantly decreases the electrical power (Fig. 7b) and, to a lesser extent, the thermal efficiency of the UNM-BRU-3 (Fig. 7a).

The nominal peak electrical power (54.2 kW_e) and peak thermal efficiency (34.5%) of the UNM-BRU-3 occurs at shaft rotation speed of 45 krpm and input thermal power to the turbine of 157 kW_{th} (Figs. 7a and 7b). Decreasing the shaft rotation speed to 30 krpm, while keeping the thermal power input to the turbine constant at 157 kW_{th}, decreases the electrical power of the UNM-BRU-3 to 39.5 kW_e (Figs. 7a and 7b). At a shaft rotation speed of 45 krpm, decreasing the thermal power input to the turbine to 100 kW_{th}, decreases the electrical power generated by the UNM-BRU-3 to 33.55 kW_e (Fig. 7b). The corresponding pressure at the exit of the compressor is 675 kPa, compared to 1.04 at the peak electrical power (54.2 kW_e). The performance results presented in Figs. 7a and 7b are for a constant compressor inlet temperature of 400 K. For the same inlet temperature, the next section investigates the effect of decreasing the inlet temperature to the turbine on the performance of the UNM-BRU-3 (Figs. 8a and 8b).

C. Effect of Decreasing the Turbine Inlet Temperature

In this section, the effect of decreasing the turbine inlet temperature from 1149 to 900 K on the performance of the UNM-BRU-3 is investigated and the obtained results are presented and discussed. The performance surfaces of the UNM-BRU-3 presented in Figs. 8a and 8b are of the thermal efficiency and the electrical power. These surfaces are made up of a grid of constant turbine inlet temperature curves of 1149, 1000, and 900 K, and intersecting curves of constant shaft rotation speeds from 30 to 55 krpm. The results presented in Figs. 8a and 8b are for a constant thermal power input to the turbine of the UNM-BRU-3 of 157 kW_{th}, an electrical alternator efficiency of 95%, and inlet temperature to the compressor of 400 K (Fig. 1).

For a given turbine inlet temperature, increasing the shaft speed decreases the pressure at the exit of the compressor $P_{(2)}$, but increases both the thermal efficiency and the electrical power of the UNM-BRU-3. They increase until reaching maximum values, then decrease with further increase in the shaft rotation speed. For the same turbine inlet temperature, the maximum thermal efficiency and electrical

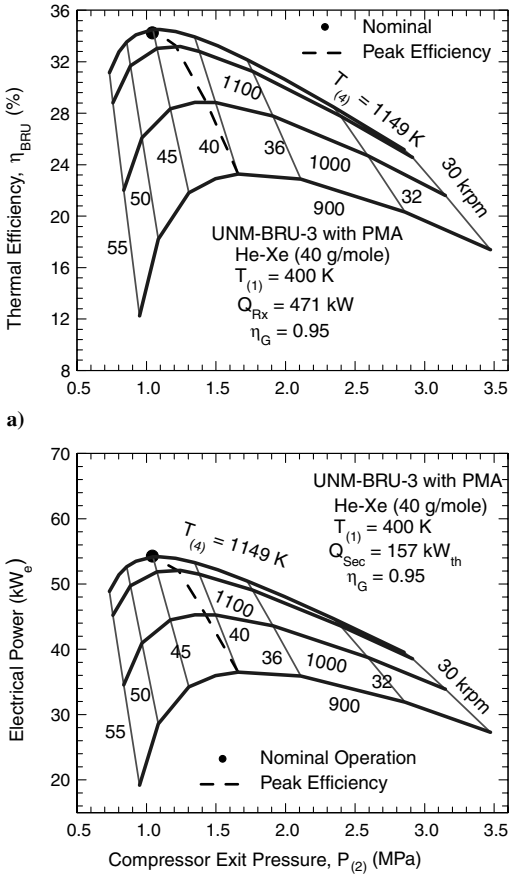

Fig. 8 Effect of turbine inlet temperature.

Table 4 Alternator dimensions and mass estimates for UNM-BRU-3

Parameter	UNM-BRU-3
Alternator dimensions	
Shaft radius, cm	2.5
Alternator rotor radius, cm	3.06
Outer alternator stator radius, cm	5.75
Alternator length, cm	15.3
Total shaft length, cm	25.3
Mass estimates	
Compressor wheel, kg	1.6
Compressor scroll, kg	8.24
Turbine wheel, kg	1.57
Turbine scroll, kg	16.31
Alternator, kg	11
Shaft, kg	1.38
Bearing, kg	6.8
Miscellaneous, kg	6.06
Total unit mass, kg	52.96

power of the UNM-BRU-3 occur at the same shaft rotation speed. This shaft rotation speed, however, decreases as the inlet temperature to the turbine decreases (Figs. 8a and 8b). However, the corresponding pressure at the exit of the compressor $P_{(2)}$ increases as the turbine inlet temperature decreases (Figs. 8a and 8b). The loci of the maximum electrical power and thermal efficiency of the UNM-BRU-3 are indicated by the dashed curves in Figs. 8a and 8b.

As indicated earlier, the peak electrical power (54.2 kW_e) and the peak thermal efficiency (34.5%) of the UNM-BRU-3 occur when the inlet temperature to the turbine is 1149 K, the shaft rotation speed is 45 krpm (Figs. 8a and 8b), and the corresponding pressure at the exit of the compressor is 1.04 MPa. For the same shaft rotation speed of 45 krpm, decreasing the turbine inlet temperature to 1000 and to 900 K decreases the maximum thermal efficiency of the UNM-BRU-3 to 28.4 and 21.8%, respectively. It also decreases the maximum electrical power generated to 44.5 and 34.2 kWe, but increases the pressure at the compressor exit to 1.43 and 1.658 MPa, respectively. The shaft speed at the maximum thermal efficiency and the maximum electrical power of the UNM-BRU-3 decreases from 45 to 40 krpm, when the inlet temperature to the turbine $T_{(4)}$ decreases from 1149 to 900 K (Figs. 8a and 8b).

A cutaway view of the assembled UNM-BRU-3 unit is shown in Fig. 9. The calculated total mass of the unit, including the PMA, is 53 kg (Table 4). This corresponds to a specific mass of 0.977 kg/kW_e (Fig. 10) when operating at the nominal conditions of a shaft rotation speed of 45 krpm, and input thermal power and inlet temperature to the turbine of 157 kW_{th} and 1149 K. This specific mass is significantly lower than those of the NASA BRU units [2,36]. At these conditions, the estimated electrical power output for the unit is 54.2 kW_e and the thermal efficiency is 34.5%. The breakdown of the masses of the various components of the UNM-BRU-3 is listed in Table 4. When operating at the same shaft rotation speed of 45 krpm and input thermal power of 157 kW_{th}, but lower inlet turbine

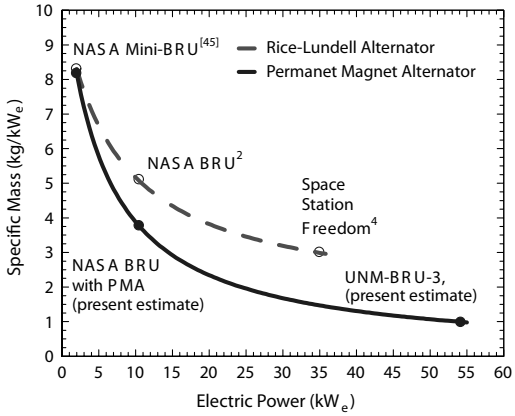

Fig. 10 UNM-BRU-3 specific mass estimate.

temperature of 900 K, the electrical power drops to 34.2 kW_e, and the hence the specific mass of the UNM-BRU-3 unit increases to 1.55 kg/kW_e.

D. Power System Prospective

A space nuclear reactor power system with three CBC loops, each with a UNM-BRU-3 and $S^{\wedge}4$ gas-cooled reactor heat source (Fig. 1), will deliver as much as 100 kW_e when operating at a total reactor thermal power of ~471 kW_{th}, turbine inlet temperature of 900 K, and shaft rotation speed of 40 krpm (Figs. 8a and 8b). The thermodynamic model of the CBC loop couples the physical models of the loop components, which include the recuperator, the gas cooler, the UNM-BRU-3 unit, and reactor core sector using the loop's overall momentum and energy balance equation. The CBC loop model accounts for the pressures losses in these components and in the connecting piping. For the space reactor power system delineated in Fig. 11, the reactor coolant and the working fluid of the CBC loops is He-Xe of 40 g/mole. The fraction of the He-Xe bled at the exit of the compressor x is used to cool the rotating shaft, including the compressor and turbine disks, the shaft bearings, and the electrical alternator. The calculated value in Fig. 11 is 2.14% of the total flow rate of the He-Xe in the CBC loop of 2.067 kg/s. The highest pressure in the loop at the exit of the compressor is 1304 KPa.

The bleed fraction is determined from the energy balance for the rotating shaft including the calculated shaft losses and the assumed losses in the electrical alternator of 5%. As indicated earlier, since the core and joules losses in the alternator change with the rotation speed of the BRU shaft, the value of the bleed fraction of the He-Xe working fluid exiting the compressor will also change (Fig. 11). However, such a change insignificantly affects the performance of the UNM-BRU-3 unit, but may change slightly the electrical power output from the alternator [15]. The temperature of the permanent magnet of the alternator is maintained constant at 500 K (~ half its curie point) using auxiliary heat pipes, heat rejection radiator, which will be designed for that purpose (Figs. 2 and 6).

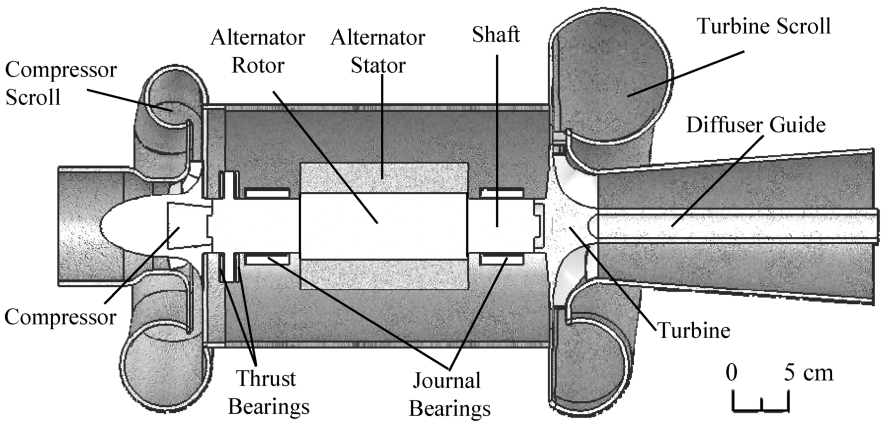

Fig. 9 A cutaway view of the assembled UNM-BRU-3.

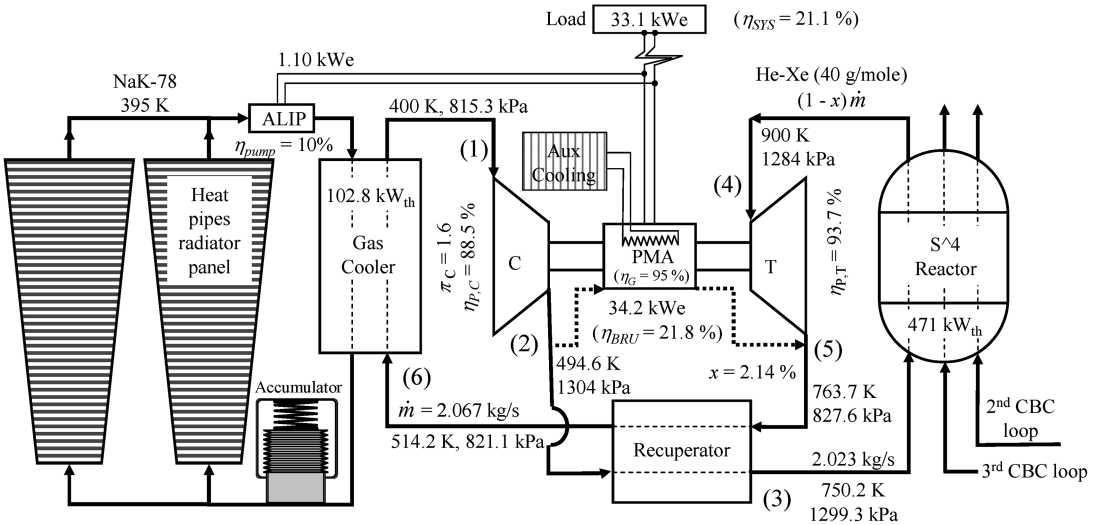

Fig. 11 Nominal operation parameters of space reactor power system with three CBC loops, each with UNM-BRU-3 operating at turbine inlet temperature of 900 K.

The relatively low reactor thermal power and turbine inlet temperature of 900 K in Fig. 11 will increase the operation lifetime and reduce the mass of the radiation shadow shield as well as the size and mass of the heat rejection radiator. The final outcome is a compact power system with a respectable thermal efficiency of ~21.1%, electrical power of ~99.3 kW_e, after accounting for the electrical power consumed by the alternating linear induction pump (ALIP) to circulate the liquid metal (NaK-78) working fluid in the heat rejection radiator panels (Fig. 11). These are in addition to a specific power greater than 30 W_e/kg (or alpha less than 34 kg/kW_e), no single point failures in reactor cooling and energy conversion, and short lead time (less than five years) for development and launch.

The highly efficient UNM-BRU-3 provides for future increases in the electrical power generated by the space reactor power system by increasing the reactor exit temperature to 1000 or 1149 K (Figs. 7 and 8), while operating at the same reactor thermal power. At these temperatures and the same shaft rotation speed of 45 krpm and the same nominal reactor thermal power of 471 kW_{th}, the thermal efficiency and the electrical power generated by the power system will be 27.5 % and 129.5 kW_e, and 33.8% and 159.2 kW_e, respectively. Many of the NASA BRU units developed in the 1970s had been tested successfully at 1149 K turbine inlet temperature for more than 35,000 h without failure or notable performance degradation [39].

IV. Conclusions

The design of the highly efficient UNM-BRU-3 has been developed at the University of New Mexico's Institute for Space and Nuclear Power Studies and optimized for He-Xe working fluid with a molecular weight of 40 g/mole, shaft rotation speed of 45 krpm, turbine inlet temperature of 1149 K, compressor inlet temperature of 400 K, and thermal power input to the turbine of 157 kW_{th}. At these operation parameters, the UNM-BRU-3 has a thermal efficiency of 34.5% and generates 54.2 kW_e at a compressor exit pressure of 1.04 MPa. In the UNM-BRU-3, the centrifugal-flow compressor and the radial-inflow turbine are mounted with a PMA on a common shaft with gas bearings. The efficiency of the PMA is taken constant at 95%, while the shaft mechanical efficiency is calculated as a function of the rotation speed. The developed performance models of the compressor and turbine for the UNM-BRU-3 have been validated successfully by comparing their predictions to those reported for NASA units built and tested in the 1960s and 1970s with different working fluids that included krypton, air, argon, and helium-xenon binary mixtures.

Also investigated are the effects on the performance of the UNM-BRU-3 of changing the shaft rotation speed from 30 to 55 krpm, the thermal power input to the turbine from 40 to 157 kW_{th}, and of decreasing the inlet temperature to the turbine from 1149 to 900 K. Results show that decreasing the shaft rotation speed significantly decreases the thermal efficiency of the UNM-BRU-3 and, to a lesser extent, the electrical power. Conversely, decreasing the thermal power input to the turbine significantly decreases the electrical power and, to a lesser extent, the thermal efficiency of the UNM-BRU-3.

At a thermal power input to the turbine of 157 kW_{th}, decreasing the shaft rotation speed to 40 krpm, decreases the thermal efficiency of the UNM-BRU-3 slightly to 33.94% and increases the compressor's exit pressure to 1.35 MPa. Further decrease in the shaft rotation speed to 30 krpm, while keeping the thermal power input to the turbine constant at 157 kW_{th}, decreases the thermal efficiency of the UNM-BRU-3 to 25.2% and increases the compressor's exit pressure to as much as 2.85 MPa. At the shaft rotation speed of 45 krpm, decreasing the thermal power input to the turbine to 100 kW_{th}, decreases the electrical power generated by the UNM-BRU-3 to 33.55 kW_e.

Results also show that decreasing the inlet temperature to the turbine decreases both the maximum thermal efficiency and electrical power of the UNM-BRU-3 and shifts them to lower shaft speed increases the pressure at the exit of the compressor. For a thermal power input to the turbine of 157 kW_{th}, decreasing the turbine inlet temperature to 1000 and 900 K decreases the maximum thermal efficiency of the UNM-BRU-3 to 28.2 and 22.57%, respectively. It also decreases the maximum electrical power to 44.27 and 35.43 kWe, but increases the pressure at the compressor exit to 1.43 and 1.658 MPa, respectively. The shaft speed at the maximum thermal efficiency and the maximum electrical power of the UNM-BRU-3 decreases from 45 to 40 krpm as the inlet temperature to the turbine decreases from 1149 to 900 K.

The maximum thermal efficiency and electrical power of the UNM-BRU-3 at a turbine inlet temperature of only 900 K are very attractive for future development of space nuclear power systems. At such relatively low turbine inlet temperature, stainless steel can be used for the reactor structure, fuel cladding, and the CBC loop piping and components. In addition to decreasing the time to deployment of the power system, the stainless steel with well-known properties and extensive operation experience will enhance the power system reliability and effectively reduce the total cost of construction and launch.

Acknowledgment

This research is sponsored by the University of New Mexico's Institute for Space and Nuclear Power Studies.

References

[1] El-Genk, M. S., "High-Energy Utilization, Dual-Mode System Concept for Mars Missions," *Journal of Propulsion and Power*, Vol. 17, No. 2,

2001, pp. 340–346.
doi:10.2514/2.5747
[2] Davis, J. E., "Design and Fabrication of the Brayton Rotating Unit," NASA CR-1870, 1972.
[3] Bents, D. J., McKissock, B. I., Withrow, C. A., Hanlon, J. C., and Schmitz, P. C., "Comparison of Dynamic Isotope Power Systems for Distributed Planetary Surface Applications," *Proceedings of the 8th Symposium of Space Nuclear Power Systems*, edited by M. S. El-Genk and M. D. Hoover, AIP Proceedings 217, American Inst. of Physics, Melville, NY, 1991, pp. 586–597.
[4] Staff of Solar Dynamic Power System Branch, "Solar Dynamic System Development for Space Station Freedom," NASA RP-1310, 1993.
[5] Harty, R., and Mason, L. S., "100-kWe Lunar/Mars Surface Power Utilizing the SP-100 Reactor with Dynamic Conversion," *Proceedings of the 10th Symposium on Space Nuclear Power and Propulsion*, edited by M. S. El-Genk and M. D. Hoover, Vol. 2, AIP Proceedings 271, American Inst. of Physics, Melville, NY, 1993, pp. 1065–1071.
[6] Barrett, M. J., and Reid, M., "System Mass Variation and Entropy Generation in 100-kWe Closed-Brayton-Cycle Space Power Systems," *Proceedings of the Space Technology and Applications International Forum (STAIF-04)*, edited by M. S. El-Genk, AIP Proceedings 699, American Inst. of Physics, Melville, NY, 2004, pp. 445–452.
[7] Gallo, B. M., El-Genk, M. S., and Tournier, J.-M., "Compressor and Turbine Models of Brayton Units for Space Nuclear Power Systems," *Proceedings of the Space Technology and Applications International Forum (STAIF-07)*, edited by M. S. El-Genk, AIP Proceedings 880, American Inst. of Physics, Melville, NY, 2007, pp. 472–482.
[8] Barrett, M. J., "Expectations of Closed-Brayton-Cycle Heat Exchanges in Nuclear Space Power Systems," *Journal of Propulsion and Power*, Vol. 21, No. 1, 2005, pp. 152–157.
doi:10.2514/1.5749
[9] Mason, L. S., Shaltens, R. K., Dolce, J. L., and Cataldo, R. L., "Status of Brayton Cycle Power Conversion Development at NASA GRC," *Proceedings of the Space Technology and Applications International Forum (STAIF-02)*, edited by M. S. El-Genk, AIP Proceedings No. 608, American Inst. of Physics, Melville, NY, 2002, pp. 865–871.
[10] El-Genk, M. S., and Tournier, J.-M., "Noble Gas Binary Mixtures for Closed Brayton Cycle Space Reactor Power Systems," *Journal of Propulsion and Power*, Vol. 23, No. 4, 2007, pp. 863–873.
doi:10.2514/1.27664
[11] Tournier, J.-M., and El-Genk, M. S., "Liquid Metal Loop and Heat Pipes Radiator for Space Reactor Power Systems," *Journal of Propulsion and Power*, Vol. 22, No. 5, 2006, pp. 1117–1134.
doi:10.2514/1.20031
[12] King, J. C., and El-Genk, M. S., "Thermal-Hydraulic Analyses of the Submersion-Subcritical Safe Space (S^4) Reactor," *Proceedings of the Space Technology and Applications International Forum (STAIF-07)*, edited by M. S. El-Genk, AIP Conference Proceedings No. 880, American Inst. of Physics, Melville, NY, 2007, pp. 261–270.
[13] El-Genk, M. S., "Space Nuclear Reactor Power System Concepts with Static and Dynamic Energy Conversion," *Energy Conversion and Management*, Vol. 49, No. 3, 2008, pp. 402–411.
doi:10.1016/j.enconman.2007.10.014
[14] Gallo, B. M., and El-Genk, M. S., "Brayton Rotating Units for Space Reactor Power Systems," *Energy Conversion and Management*, Vol. 50, No. 9, 2009, pp. 2210–2232.
doi:10.1016/j.enconman.2009.04.035
[15] Yoder, G. L., Carbajo, J. J., Murphy, R. W., Qualls, A. L., Sulfredge, C. D., Moriarty, M. P., Widman, F. J., Metcalf, K. J., and Nikitkin, M., "Technology Development Program for an Advanced Potassium Rankine Power Conversion System Compatible with Several Space Reactor Designs," Oak Ridge National Lab. Rept. TM-2004/214, 2004.
[16] AiResearch, "Design and Fabrication of the Brayton Cycle Turbine Research Package," NASA CR-54367, 1965.
[17] Dunn, J. H., "Post Test Inspection of Three Brayton Rotating Units," International Energy Conversion Engineering Conf., Paper 719030, 1971.
[18] Whitfield, A., and Baines, N. C., *Design of Radial Turbomachinery*, Longman Scientific & Technical, London, 1990.
[19] Aungier, R. H., *Centrifugal Compressors*, American Society of Mechanical Engineers Press, New York, 2000.
[20] Aungier, R. H., *Turbine Aerodynamics*, American Society of Mechanical Engineers Press, New York, 2006.
[21] Aungier, R. H., "Mean Streamline Aerodynamic Performance Analysis of Centrifugal Compressors," *Transactions of the ASME: Journal of Turbomachinery*, Vol. 117, July 1995, pp. 360–366.
doi:10.1115/1.2835669
[22] Coppage, J. E., Dallenbach, F., Eichenberger, H. P., Hlavaka. G. E., Knoernschild, E. M., and Van Lee, N., "Study of Supersonic Compressor for Refrigeration and Pressurization Systems," Wright Air Development Center TR 55-257, 1956.
[23] Galvas, M. R., "FORTRAN Program for Predicting Off-Design Performances of Centrifugal Compressors," NASA TN D-7487, 1973.
[24] Schlichting, H., *Boundary-Layer Theory*, 7th ed., McGraw–Hill, New York, 1979.
[25] Johnston, J. P., and Dean, R. C., "Losses in Vaneless Diffusers of Centrifugal Compressors and Pumps: Analysis, Experiment, and Design," *Transactions of the ASME: Journal of Engineering for Power*, Vol. 88, 1966, pp. 49–62.
[26] Jensen, W., and Sunderland, P. B., "Off-Design Performances Predictions of Centrifugal Pumps," *Proceedings of the ASME Winter Annual Meeting*, American Society of Mechanical Engineers, Fairfield, NJ, 1990, pp. 1–10.
[27] Stanitz, J. D., "One-Dimensional Compressible Flow in Vaneless Diffuser of Radial- and Mixed-Flow Centrifugal Compressor Including Effects of Friction, Heat Transfer and Area Change," NACA TN 2610, 1952.
[28] Balje, O. E., "A Contribution to the Problem of Designing Radial Turbomachines," *Transactions of the ASME*, Vol. 74, No. 1, 2006, pp. 451–742.
[29] Meitner, P. L., and Glassman, A. J., "Computer Code for Off-Design Performance Analysis of Radial-Inflow Turbines with Rotor Blade Sweep," NASA TP 2199, 1983.
[30] Daily, J. W., and Nece, R. E., "Chamber Dimension Effects on Induced Flow and Frictional Resistance of Enclosed Rotating Disks," *Transactions of the ASME, Series D: Journal of Basic Engineering*, Vol. 82, 1960, pp. 217–232.
[31] Roelke, R., "Miscellaneous Losses, in Turbine Design and Application," edited by A. J. Glassman, NASA SP-290, Vol. 2, 1973, pp. 125–48.
[32] Howard, A. H., Brunckner, R. J., DellaCorte, C., and Radil, K. C., "Gas Foil Bearing Technology Advancements for Closed Brayton Cycle Turbines," *Proceedings Space Technology and Applications International Forum (STAIF-07)*, edited by M. S. El-Genk, AIP Proceedings No. 880, American Inst. of Physics, Melville, NY, 2007, pp. 668–680.
[33] Eckardt, D., "Instantaneous Measurements in the Jet-Wake Discharge Flow of a Centrifugal Compressor Impeller," *Transactions of the ASME: Journal of Engineering for Power*, Vol. 97, 1975, pp. 337–346.
[34] Eckardt, D., "Detailed Flow Investigations Within a High-Speed Centrifugal Compressor," *Journal of Fluids Engineering*, Vol. 98, 1976, pp. 390–402.
[35] Japikse, D., "A Critical Evaluation of Three Centrifugal Compressors with Pedigree Data Sets, Part 5: Studies in Component Performance," *Transactions of the ASME: Journal of Turbomachinery*, Vol. 109, 1987, pp. 1–9.
[36] Repas, D. S., and Edkin, R. A., "Performance Characteristics of a 14.4-Kilovolt-Ampere Modified Lundell Alternator for 1200 Hz Brayton-Cycle Space-Power System," NASA TN D-5405, 1996.
[37] AiResearch, "Final Report 1200-Hz Brayton Electrical Research Components," NASA CR-72564, 1969.
[38] Patrick, D. R., and Fardo, S. W., *Rotating Electrical Machines and Power Systems*, Prentice–Hall, Upper Saddle River, NJ, 1985.
[39] Ashe, T. L., and Otting, W. D., "Brayton Power Conversion System Parametric Design Modeling for Nuclear Electric Propulsion," NASA CR-191135, 1993.
[40] Campbell, P., *Permanent Magnet Materials and Their Applications*, Cambridge Univ. Press, New York, 1994.
[41] Levi, E., *Polyphase Motors: A Direct Approach to Their Design*, Wiley, New York, 1984.
[42] Mason, L. S., Shaltens, R., and Espinosa, W. D., "Experimental Data for Two Different Alternator Configurations in a Solar Brayton Power System," NASA TM-107509, Rept. E-10811, 1997.
[43] Halsey, D. G., and Fox, D. A., "Closed Brayton Cycle (CBC) Power Generation from an Electric System Perspective," *Proceedings of the Space Technology and Applications International Forum (STAIF-06)*, edited by M. S. El-Genk, AIP Proceedings No. 813, American Inst. of Physics, Melville, NY, 2006, pp. 662–672.
[44] Kenny, B. H., and Tokars, R. P., "Feasibility Study of Jupiter Icy Moons Orbiter Permanent Magnet Alternator Start Sequence," Rept. 15391, NASA/TM-2006-214034, 2006.
[45] Birchenough, A. G., "The 2 kW Mini-BRU Electrical Controls Concept and Transient Performance," NASA Rept. TM-2006-214034, 2006.
[46] Dobler, F. X., "Mini-BRU/BIPS 1300 Watte Dynamic Power Conversion System Development," NASA Rept. CR-159440, 1978.

G. Spanjers
Associate Editor